Proceedings of the ASME 2010 29th International Conference on Ocean, Offshore and Arctic Engineering
OMAE2010
June 6-11, 2010, Shanghai, China

OMAE2010-20662

DYNAMIC ANALYSIS OF RISER RELEASE AND LOWERING

Sampath Atluri, Nicole Liu, Anil Sablok, Tim Weaver
Technip, Houston, Texas 77079, USA

ABSTRACT
Oil and gas development in certain harsh environments, such as extreme storm prone areas or arctic regions, may require the floating production platform to be designed to enable it to be released from its risers and moorings and moved out of the way of the approaching threat. Such floating platforms generally employ an underwater disconnectable buoy to support the moorings and risers after the main platform is moved away. For a deep draft floating structure, the risers can be released from their support near the top of the platform and lowered through the hull to a disconnectable buoy. In such a case, the risers can be routed through I-tubes and lowered in a controlled manner using rigging during a normal release operation. However, an emergency disconnection may require lowering of the risers without guidance of rigging. To avoid damage to the risers and the buoy during the emergency disconnection, risers can be fitted with passive damping devices to limit the lowering riser speed. This paper presents the numerical efforts to define the emergency riser release and lowering procedure.

CFD simulations were performed to evaluate the hydrodynamic behavior of a disconnected riser in a flooded I-tube with the controlling devices attached to the risers. Applying the CFD results, riser lowering performance was computed using finite element analysis method. Primary parameters that affect flexible riser behavior, including stress level and curvature, are identified and sensitivity study results are presented. This paper concludes that a safe and controlled riser release procedure and system is achievable.

1. INTRODUCTION
An underwater disconnectable keel buoy could be used in harsh environments to support mooring and flexible riser systems when riser and mooring systems need to be disconnected from the main platform to move the main platform out of the way of the approaching threat. During an emergency, the allowable time to disconnect may be no more than about fifteen minutes. This time limit rules out the option of using a winch or other equipment to lower the riser system, which is rather complex and relatively slow.

A riser configuration that can be quickly disconnected is shown in Figure 1. The riser is hung-off near the top of the hull and runs vertically through a tube within the floating structure before exiting at the bottom of the keel buoy. It then hangs in a catenary configuration below the keel buoy before returning to a support chute fitted to the keel buoy. From the support chute, the riser descends to the seafloor. Valves at the top of the riser confine the contents and prevent spills during disconnection.

When the riser is released from its hang-off location, the upper section falls freely through the vertical tube and increases the length of riser hanging below the keel buoy as shown in Figure 2. When the top of the riser reaches the keel buoy, it is caught by a stopper. To control the speed of the free fall and prevent damage to the riser from high compression and uncontrolled bending, passive damper devices are attached to the upper riser section to allow a feasible and safe disconnection. After all the risers have been released and are supported by the keel buoy, the main structure is released from the keel buoy and moved to a safe location.

This paper presents the numerical investigation on the feasibility of the riser system being released from its hang-off location near top of the hull and falling “freely” to the bottom of the keel buoy. CFD analysis was conducted to understand the hydrodynamic behavior of the riser with the dampers. CFD simulations show that a damper configuration with desirable hydrodynamic behavior is designable. Different passive damper arrangements studied using CFD analysis and the riser lowering analyses are discussed in the following sections.

Key parameters that affect the riser descending procedure were studied. Numerical results using different FEA software were also compared.

2. NOMENCLATURE

ρ	Density of sea water
v	Velocity of the riser (m/s)
A_p	Projected area (for drag coefficient calculation)
F_d	Drag force (N)
OD	Outer diameter (m)
ID	Inner diameter (m)
E	Elastic Modulus
A	Area of cross section
I	Area moment of inertia
L	Length (m)
C_d	Drag Coefficient
CFD	Computational Fluid Dynamics
MWL	Mean water line
MBR	Minimum Bend Radius

3. CFD SIMULATIONS

The objective of the CFD calculations was to identify the most suitable damper configuration by estimating the drag coefficient of the passive damping devices fitted to the riser. Figure 3 shows a schematic of one such damping device configuration with four baffles. The CFD analysis was done in 3D. As the riser descends through the I-tube, the damping device (referred to as a 'pig' henceforth due to its resemblance with the pipeline service pigs) will constrict the annulus between the riser and the outer pipe. Drag properties of the pig change with the number of baffles used, their size and spacing. For the current analysis, only a short section of the riser fitted with a pig at its center is considered. The simplified schematic is shown in Figure 4. Note that the aspect ratio in the figure is altered for readability. The length of the riser modeled is 8 m (with the pig fitted at its center) and the length of the outer pipe (I-tube) is 150 m. Riser length has been verified to be sufficiently long to not alter the solution. The purpose of the study was to find the drag coefficients of the pig only.

At the start of the simulation, the riser and the pig are completely immersed in water near the top end of the I-tube. Then the riser and the pig are forced to descend through the I-tube at a specified constant velocity. It is assumed that the pig never touches the outer pipe throughout its descent. No-slip wall boundary conditions are applied on the riser, pig and the surrounding outer pipe. A non-zero velocity specification on the riser and the pig, free surface condition at the top of the water column and standard outflow (open pipe) at the bottom of the I-tube are applied. Hydrostatic pressure is applied throughout the water column. As the pig descends, the flow in the annulus between the pig and the outer pipe can be considered to be a combination of Couette flow and Poiseulle flow with changing pressure gradient due to the expected leakage through the bottom of the I-tube. The Reynolds number for this type of flow is based on the size of the annulus and the velocity of the descent of the inner pipe. For the simulations reported here, the Reynolds number is around 25,000. This is significantly higher than the transition Reynolds numbers for either Couette or Poiseulle flows [1]. Hence, RANS turbulence modeling based on the Spalart-Allmaras one-equation model [2] was used to calculate turbulence. The mesh used is made of isotropic tetrahedral elements except for the boundary layer region with non-isotropic tetrahedral elements. Wall functions were applied for near wall turbulence. The average surface y+ monitored for all the reported results is about '20'. Mesh points in the flow domain are allowed to move only in the axial direction and slide down along the walls of the outer pipe. Mesh motion is accomplished by the Arbitrary Lagrangian-Eulerian (ALE) method. However, mesh points in the vicinity of the riser are forced to move along with the riser to preserve the quality of the mesh in the region of interest. This specification results in a non-deforming mesh region close to the riser and the pig, an expanding mesh region above it and a contracting mesh region below it. The difference between the mesh at the beginning and the end of the simulation is illustrated in Figure 5.

As the pig moves with the riser, the drag force on the pig is recorded. This force becomes steady after all the transient effects die out. The pig pushes water out through the bottom of the outer pipe which makes the free surface at the top descend in the same direction as the pig. Once the drag force becomes steady, the elevation of the free surface remains constant and very little mass flow occurs through the bottom. This is illustrated in Figure 6. The total force acting on the pig (only) as it descends along the I-tube is also shown in Figure 6. The force becomes steady after descending about half the length of the I-tube indicating that the pig has reached its terminal velocity. Figure 7 shows the instantaneous velocity field around the pig. A non-dimensional force coefficient (drag coefficient, C_d, in this case) is then calculated as follows:

$$C_d = F_d / \left(0.5 * \rho * v^2 * A_P\right)$$

Here

F_d is total drag force on the pig in the direction of motion. For multiple baffles, total force on all the baffles is used. A_P is the projected area of the pig (only).

Table 1 summarizes the results for various pig configurations investigated. The drag coefficient on the pig reduces with increasing annulus size (gap between the outer end of the pig and the I-tube changed from 25 mm to 51 mm). This is true for single or multiple baffles as evident from Cases 1 to 5 in the table. Increasing space between the baffles results in increase of the drag coefficient, compare Case 5 and Case 6. The drag coefficient remains the same even if the prescribed velocity of descent is doubled which may suggest that the drag coefficient

is independent of Reynolds number. Based on the estimated C_d values, ease and feasibility of arrangement, an ideal pig configuration is chosen for further analysis described in the following sections.

All the CFD analyses were done using Finite Element CFD code AcuSolve™. It is based on a Galerkin Least-Squares formulation. It uses a fully coupled pressure-velocity iterative solver and a generalized alpha method as a semi-discrete time stepping algorithm. AcuSolve™ is second order accurate in time and space. Typical mesh point count for the analysis is in the order of one million. The simulations were carried out on a parallel cluster and a runtime of about 5 hours for 1000 time steps (complete simulation) is recorded using 64 processors. Mesh size sensitivity and time step sensitivity were performed prior to the analysis. Force on the pig was compared for the different sensitivity cases studied and is shown in Figure 8 and Figure 9.

4. RISER RELEASE AND LOWERING ANALYSIS

4.1 Modeling

In the riser disconnection analysis, only the upper riser section was modeled as shown in Figure 10, since the lower section remains stationary. The riser connect/disconnect interface was located 15.5 m above the mean water line (MWL) and 4.0 m above the top of the vertical I-tube. The bottom of the keel buoy was 171.0 m below MWL. The horizontal distance between the center of the vertical tube and the riser lower end was 33.0 m. Two centralizers were attached to the riser. One was placed at the top of the 1st valve, which was 0.6 m from the riser top, and the other was placed right below the 2nd valve. The two valves were adjacent to each other. The two centralizers were used to keep the valves straight during the descent. The drag contribution of the centralizers is not significant compared to that of the passive dampers. Two dampers were employed, located at 7.2 m above MWL and 7.8 m below MWL, respectively in the connected condition.

The riser system properties used in the analysis are summarized in Table 2. Both the centralizers and dampers had a 51 mm gap to the vertical tube wall. The analysis was done for two extreme riser conditions: empty and flooded with water.

The hydrodynamic coefficients used for the riser are summarized in Table 3. The drag coefficients used for the dampers are based on CFD results. The same axial drag coefficient was applied to both dampers.

4.2 Results

A series of snapshots of the riser without any dampers attached free falling through the vertical tube after being disconnected from its hang-off location are shown in Figure 11. With no constraints or damping devices other than the friction between the riser and tube inside wall, analysis indicated that riser would experience high compression and uncontrolled damping. Passive dampers were introduced to reduce the compression and control bending by providing high axial drag loads. Figure 12 shows a series of snapshots typical of the riser with dampers free falling through the vertical tube after being disconnected. According to the CFD analysis, the damper configuration can be designed to achieve a desired hydrodynamic behavior to control the riser system releasing behavior.

Drag Coefficient Effects

To estimate the effects of the damper design and drag on the descending riser, riser minimum bend radius (MBR) was computed with three different damper configurations. The axial drag coefficient of each damper configuration was different, while the cross section area was the same. The results are shown in Figure 13. Envelope for MBR is plotted along the length of the riser (measured from the top of the riser) for each damper configuration. These drag coefficient sensitivity simulations were conducted in calm water condition for a riser flooded with sea water, which is conservative when compared to an empty or gas-filled riser. Results show that the riser MBR is affected by the damper drag properties and quickly converges as the effective drag coefficient becomes higher than 10. It may be noted from Figure 13 that there are two sections along the length of the riser showing relatively smaller bend radii compared to the rest of the riser. The first section/region is located between the 2nd centralizer (3 m from riser top) and 2nd damper (23 m from riser top). The small bend radius in this section can be attributed to the high bending moment caused by the weight of the valve at the riser top. The second section with small bend radius is located between 143 m and 234 m, measured from the top. This section corresponds to the sag point which is the lowest hanging section between the chute and keel buoy (refer Figures 1&2). Initially the sag point is located 234 m from the top. With the riser top descending, the arc length between the sag location to the chute is increasing, and the length measured from the top to sag location keeps decreasing until the riser is stopped at the keel buoy. The sag point moves from its initial location of 234 m to a final location of 143 m measured from the riser top in the releasing process. The minimum bend radius at the sag location occurred when the riser comes to rest at the keel buoy.

Figure 14 shows time histories of the riser top vertical velocity with different damper drag coefficients. The time histories show that riser falling velocity increased sharply to a maximum value before the top of the riser entered the I-tube. As the riser descended along the tube, its free fall velocity gradually decreased until the exit, where the riser was quickly stopped. Though riser MBR becomes insensitive with damper drag coefficients higher than 10, the riser terminal velocity is still affected by high drag coefficients. The terminal velocity is reduced from 2.56 m/s to 1.89 m/s, as the drag coefficient is increased from 55 to 100. Correspondingly, the riser system releasing time is affected by the damper drag coefficient as well. The controlled release riser disconnection procedure is

around 60-100 sec which is consistent with the time frame requirements for an emergency disconnection procedure.

Riser Weight Effects

Using two of the 4-baffle dampers, each with a drag coefficient of 100, riser releasing was simulated in both the void and flooded conditions. The wet weight ratio between the void and flooded riser is 0.6.

Results show that a lighter riser weight has a slower falling speed as shown in Figure 15. Both descent times are acceptable, so the same damper configuration can be used for both riser conditions. Riser MBR was hardly changed by the riser weight.

Platform Motion Effects

Since the platform would likely experience motions due to the environmental conditions when an emergency disconnection becomes necessary for the riser system, a static 5-degree platform pitch angle was applied in the riser releasing simulation. Figure 16 shows that the minimum riser bend radius occurred at the same two locations with different platform pitch and therefore the effect of platform pitch is insignificant. The first location is governed by the weight of the valve and the second location by the riser sag point. However, the riser bend radius at other locations is decreased by the platform pitch.

Comparisons between Orcaflex and Abaqus

All of the riser release and lowering analysis results presented above were computed using Orcaflex in time domain. To verify the validity of the numerical simulations, a different finite element analysis software, ABAQUS, was used.

A separate riser model was built using ABAQUS to simulate the riser releasing process. Two 4-baffle dampers, each with a drag coefficient of 80, were investigated. The simulation was performed in calm water condition with the riser flooded with sea water. The results based on the two software are shown in Figure 17 and Figure 18. Comparisons of the results show very good agreement between the different software.

5. CONCLUSIONS

1. The feasibility of the application of a riser lowering system design has been demonstrated with a combination of CFD and FEA analyses.
2. Damping characteristics of the dampers were evaluated with CFD.
3. Dampers helped to slowdown the riser descent avoiding high riser compression, uncontrolled bending and landing impact.
4. The descent can be controlled as required by changing the geometry of the dampers
5. Good agreement was found for FEA analysis using two different software.
6. Safe and controlled riser release procedure by adding damping devices is achievable.

6. REFERENCES

1. Frank M. White, “Viscous Fluid Flow”, McGraw-Hill publications, 2nd Edition.
2. Spalart, P.R. and Allmaras, S.R. “A one-equation model for aerodynamic flows”, AIAA 92-0439.
3. OrcaFlex User Manual, April 2007.

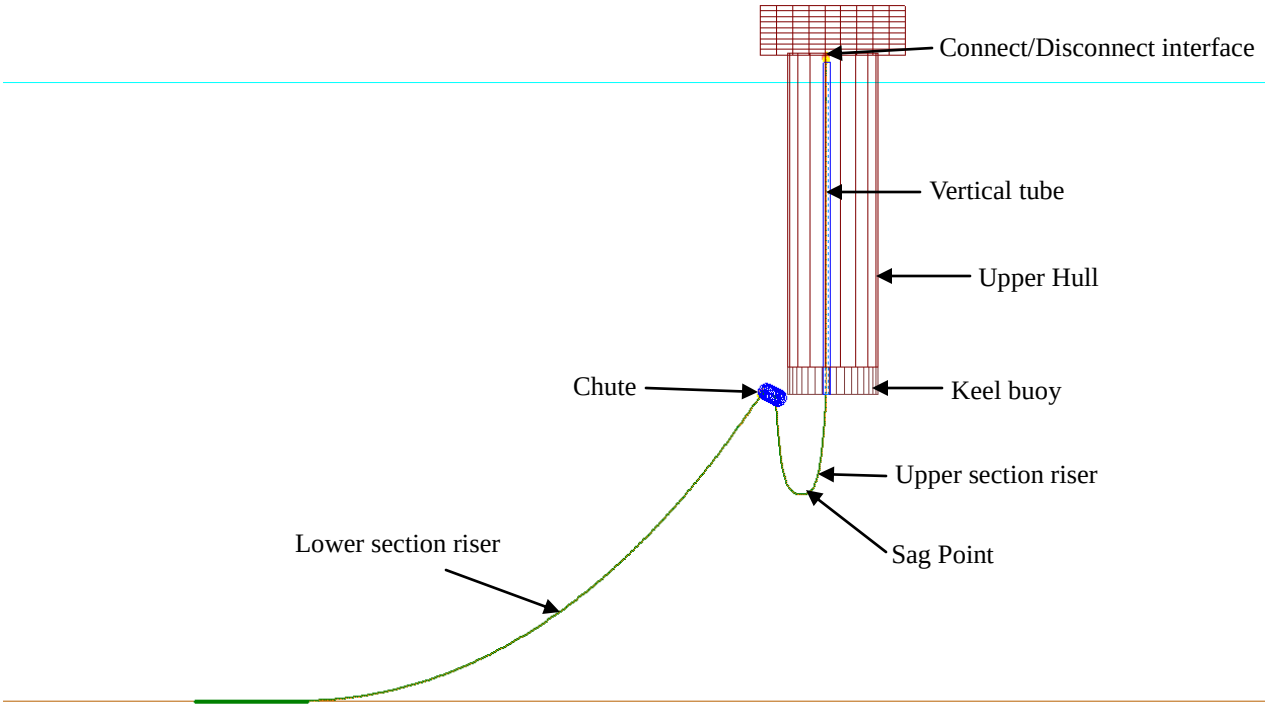

Figure 1 Normal Riser Profile

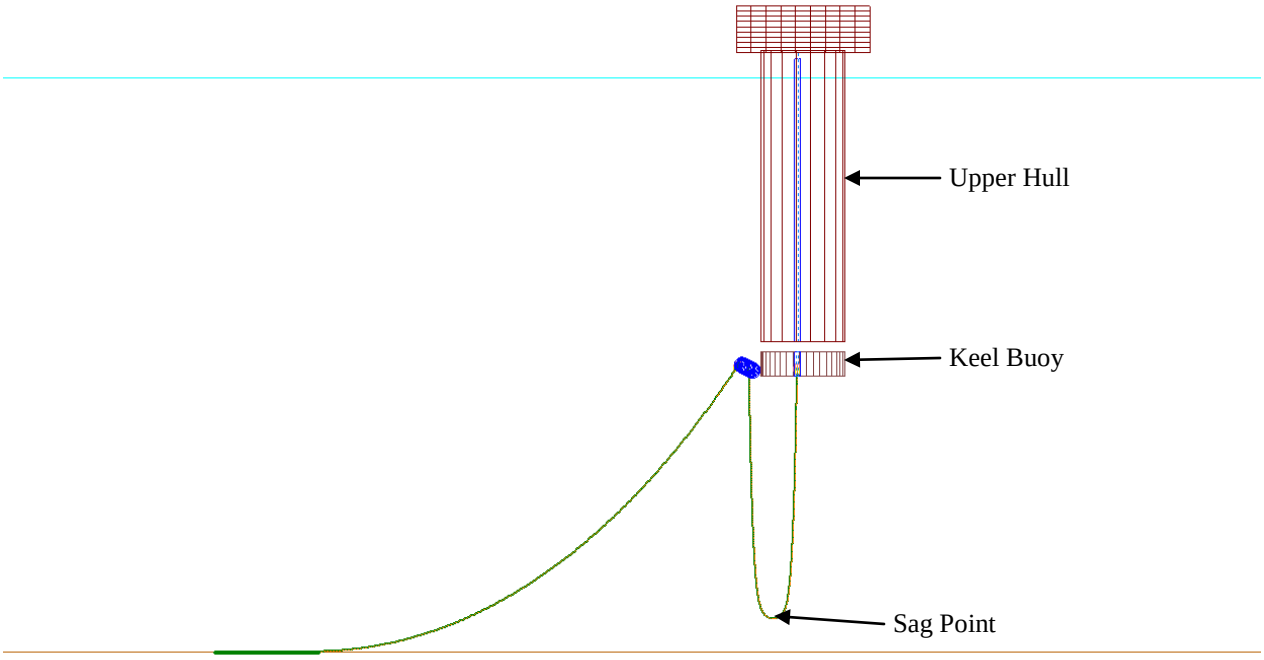

Figure 2 Disconnected Riser Profile

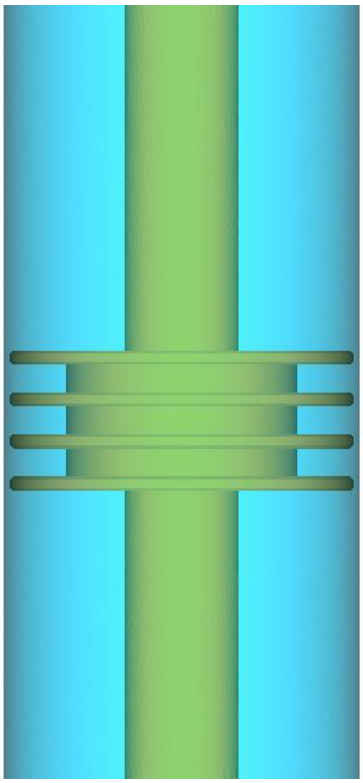

Figure 3 Geometry of the Riser Fitted with a Damping Device Inside the Vertical I-Tube

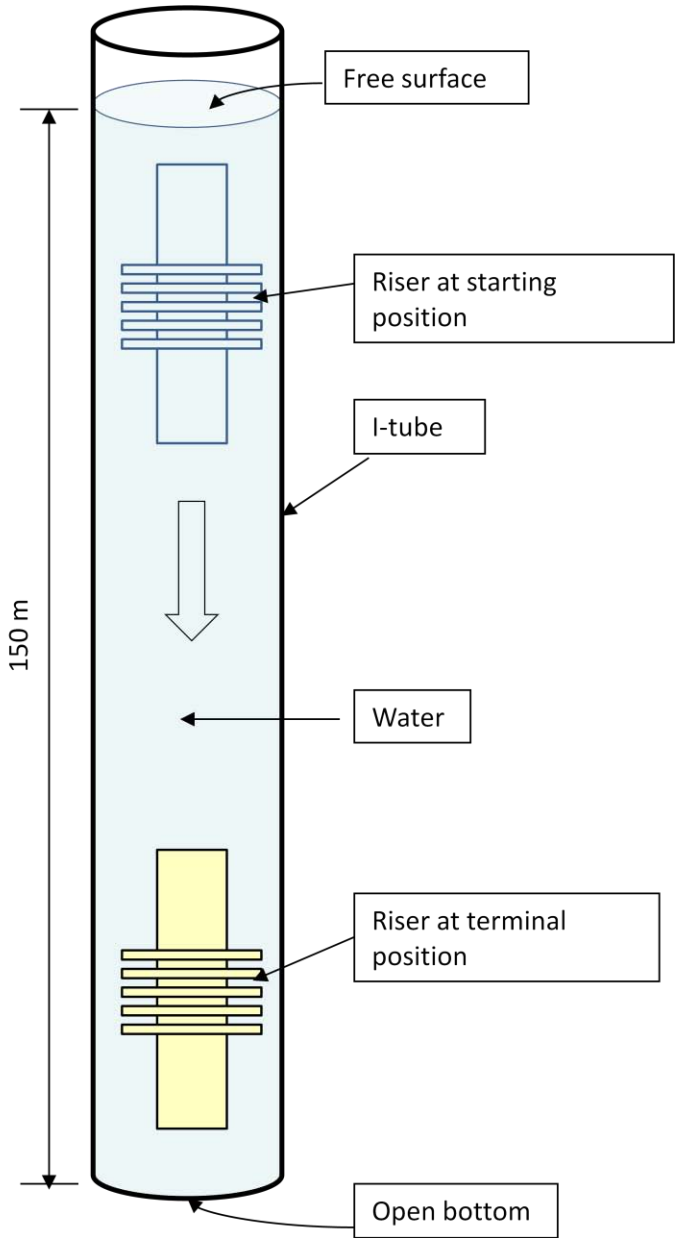

Figure 4 Simplified View of the Geometry

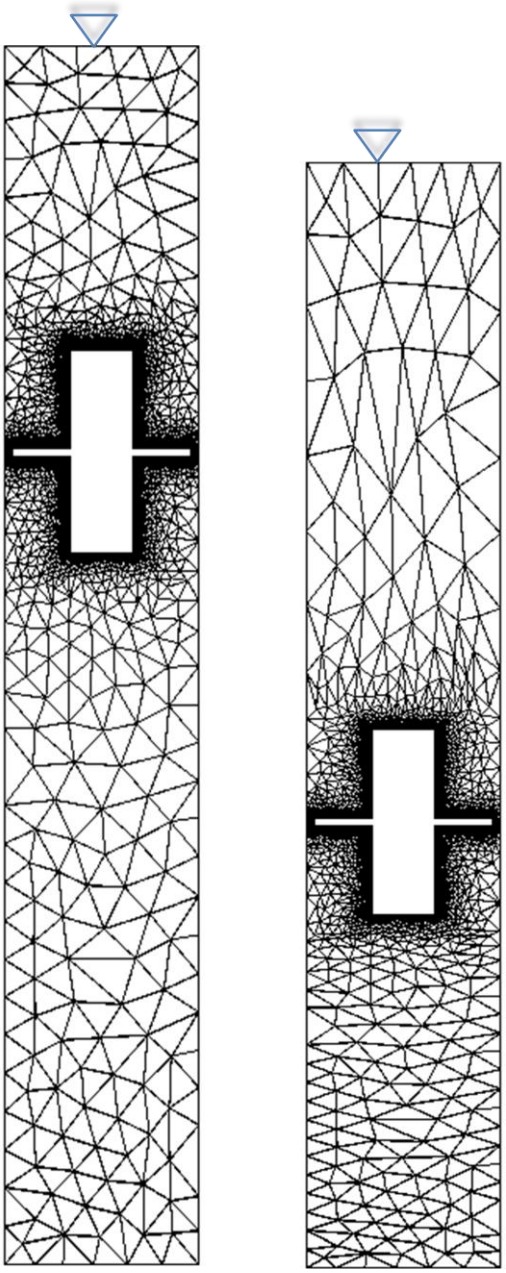

Figure 5 Mesh Before and After Deformation (scale altered for readability)

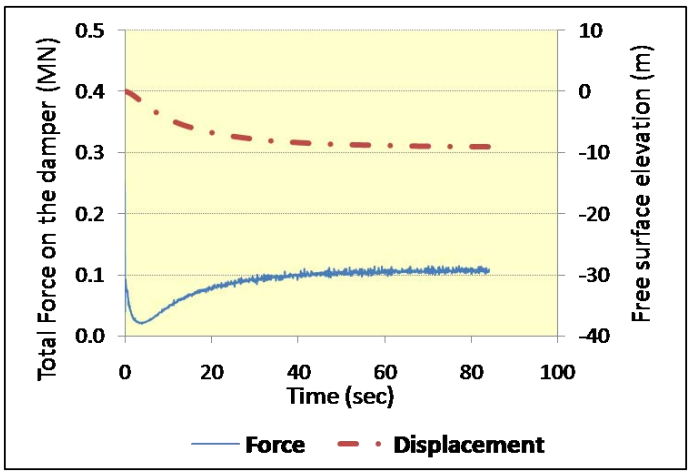

Figure 6 Force on the Pig/Damper During Descent

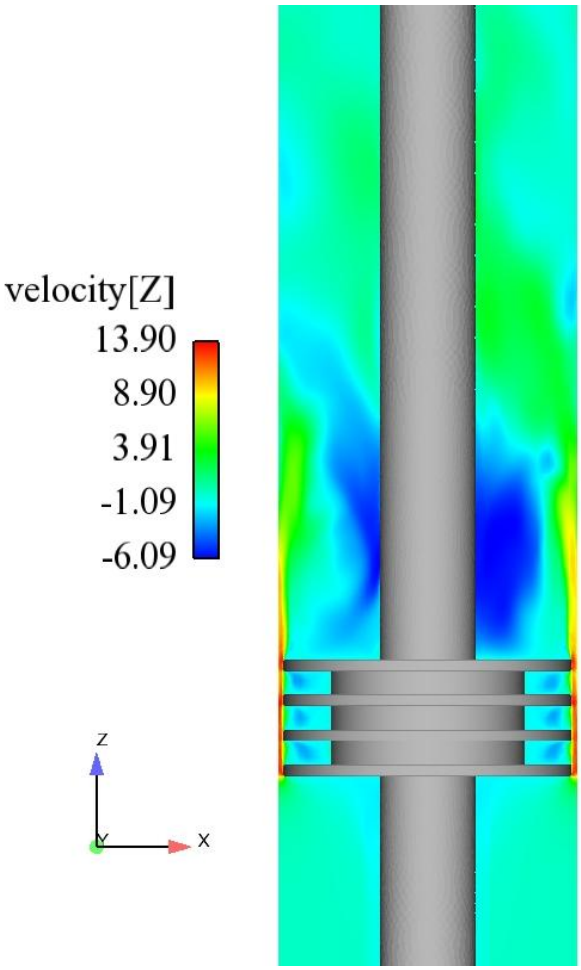

Figure 7 Instantaneous Velocity (noramlized with the riser descent velocity) During Descent

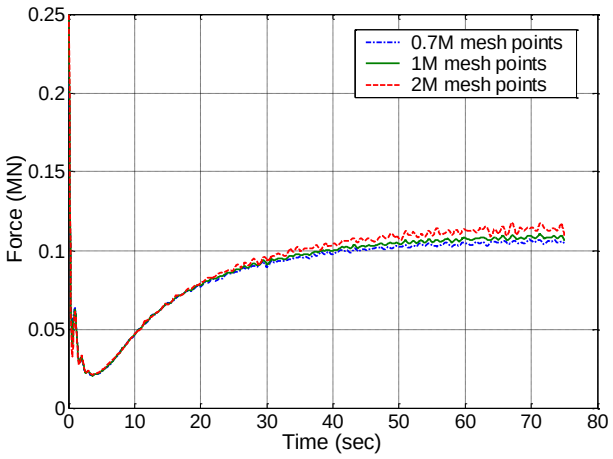

Figure 8 Mesh Sensitivity on Drag Force

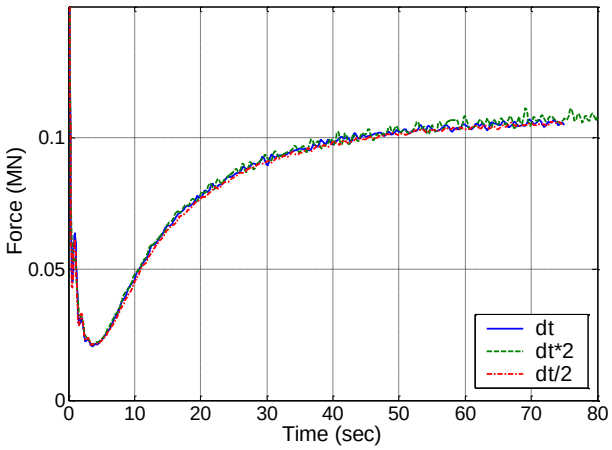

Figure 9 Time Step Sensitivity on Drag Force

Table 1 Drag Coefficient for Different Pigs/Dampers

Case	Model	No. of baffles per pig	Vel. of pig (m/s)	Size of annulus (mm)	Spacing between baffles (mm)	Cd
1		1	1	25.4	0	**194**
2		1	1	50.8	0	**58.5**

Case	Model	No. of baffles per pig	Vel. of pig (m/s)	Size of annulus (mm)	Spacing between baffles (mm)	Cd
3		1	2	50.8	0	**56**
4	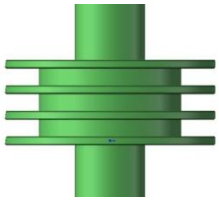	4	1	25.4	101.6	**283**
5	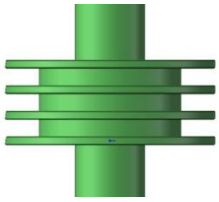	4	1	50.8	101.6	**62**
6	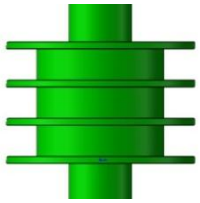	4	1	50.8	203.2	**80**
7		4	1	50.8	101.6/1295.4	**101**

Table 2 Riser System Properties

Flexible riser				
OD	ft	1.394	m	0.425
ID	ft	1.001	m	0.305
Weight in air	lb/ft	173	kg/m	258
Length	ft	890.37	m	271.39
Contents		Empty/sea water		Empty/sea water
EA	kips	2.086E5	kN	928E3
EI	Kips-ft^2	605	kN-m^2	250
Valve				
OD	ft	2.625	m	0.8
ID	ft	1.001	m	0.305
Weight in air	kips	7.43	te	3.372
Length	ft	3.28	m	1.0
Centralizer				
OD	ft	4.098	m	1.249
Damper				
OD	ft	4.098	m	1.249
ID	ft	1.394	m	0.425
L	ft	9	m	2.74
Density	lb/ft^3	95.051	kg/m^3	1522
Vertical tube				
ID	ft	4.265	m	1.3

Table 3 Riser Hydrodynamic Coefficients

Hydrodynamic Coefficients	Value
Drag Coefficient, Normal	0.7
Drag Coefficient, Axial	0.0
Added Mass, Normal	1.0
Added mass, Axial	0.0

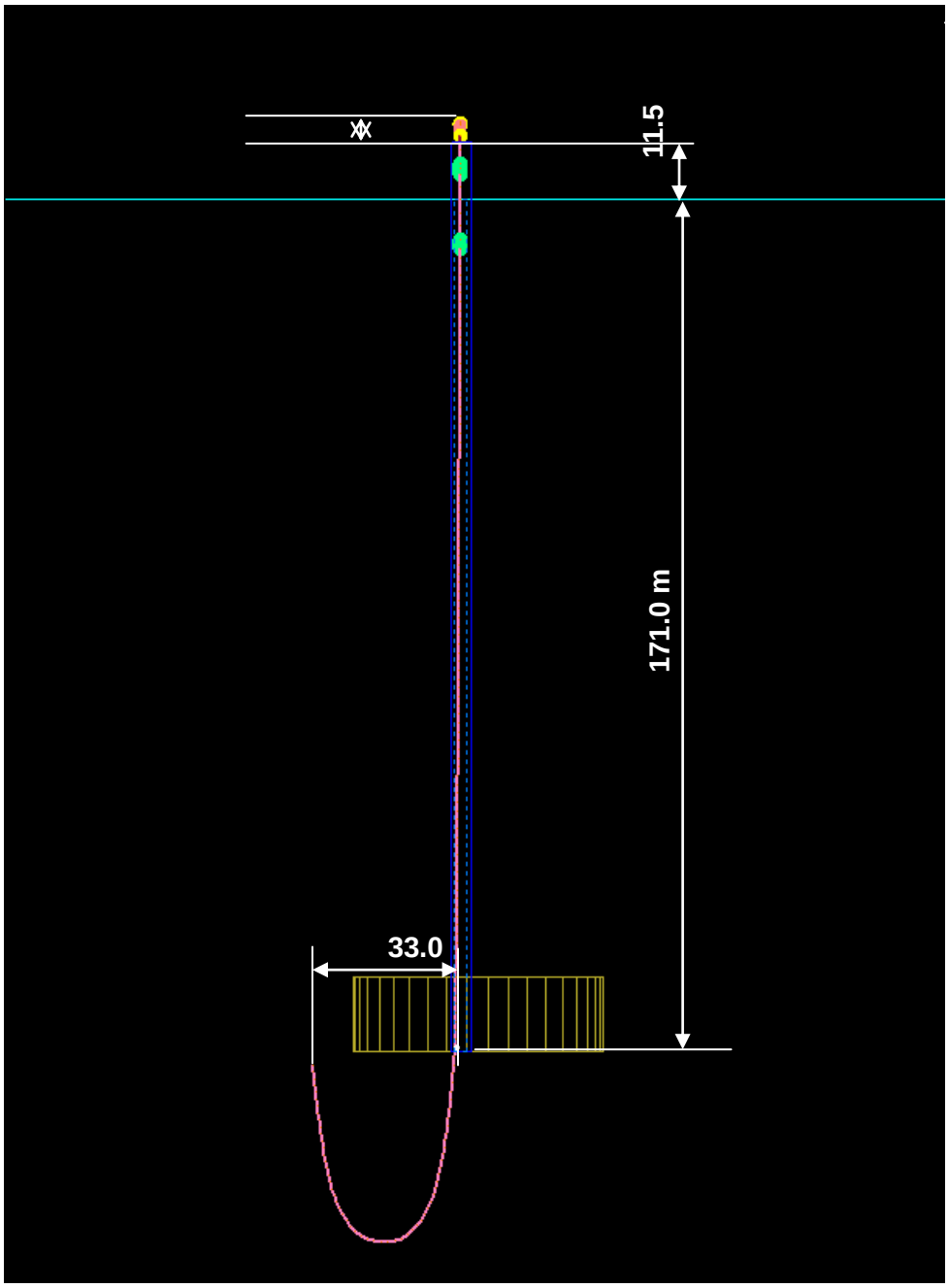

Figure 10 Riser Model

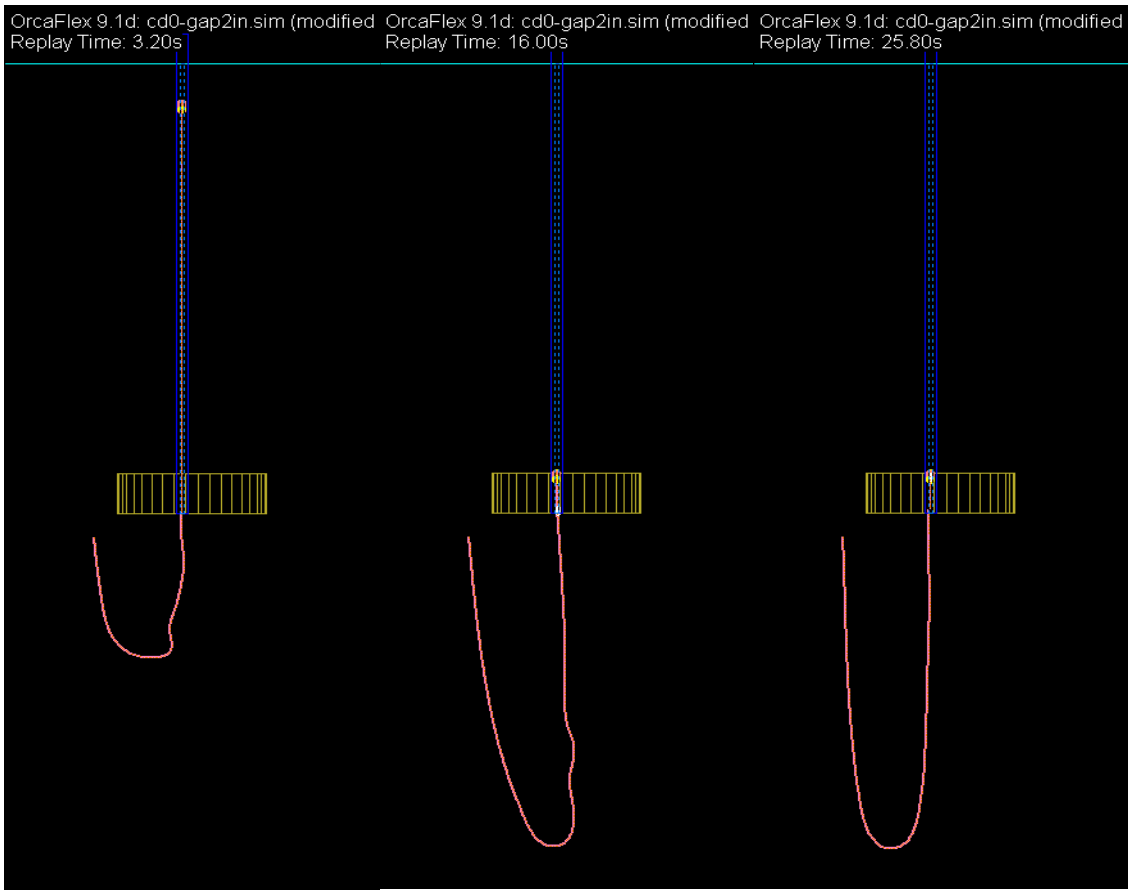

Figure 11 Snapshots of Riser Configuration During Release without Damper

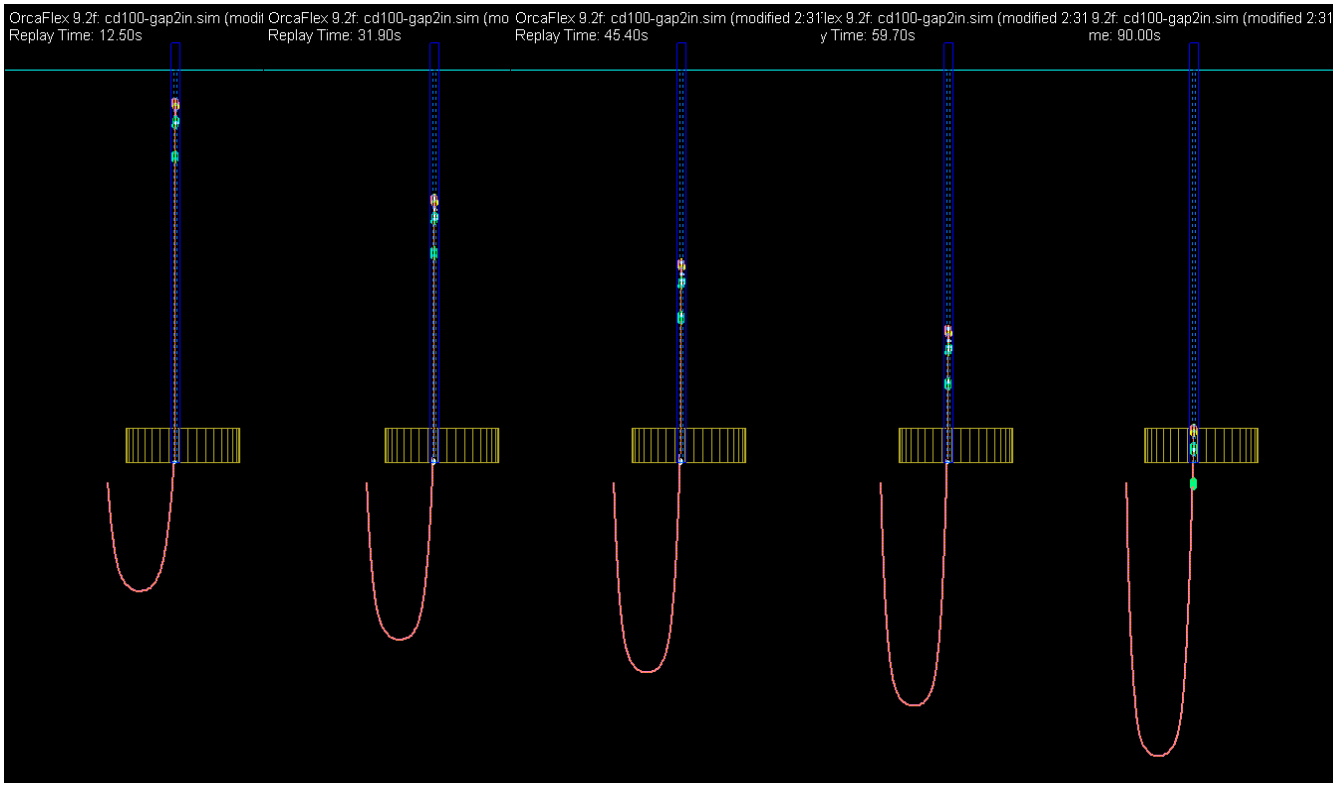

Figure 12 Snapshots of Riser Configuration During Release with Damper

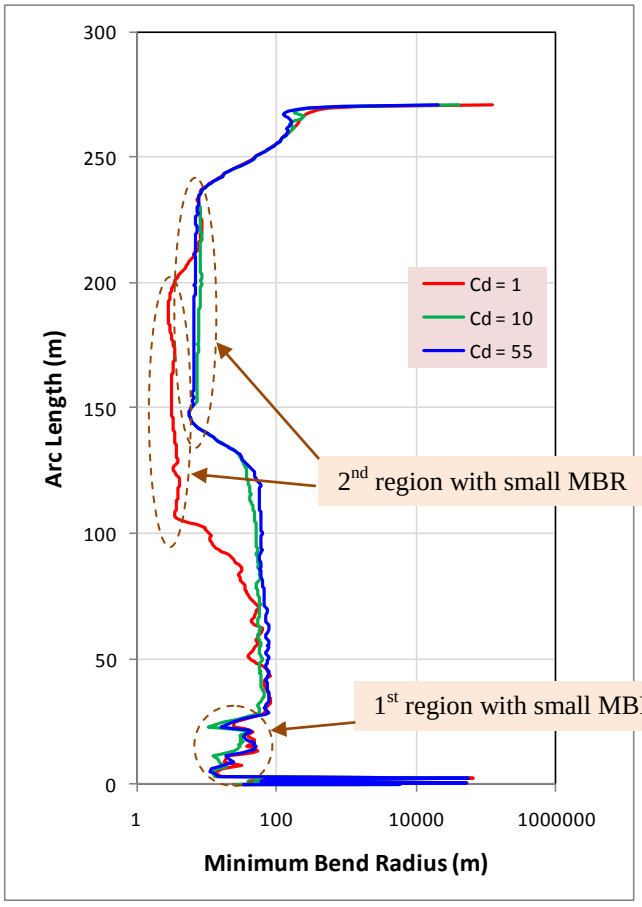

Figure 13 Minimum Bend Radius Variations with Damper Drag

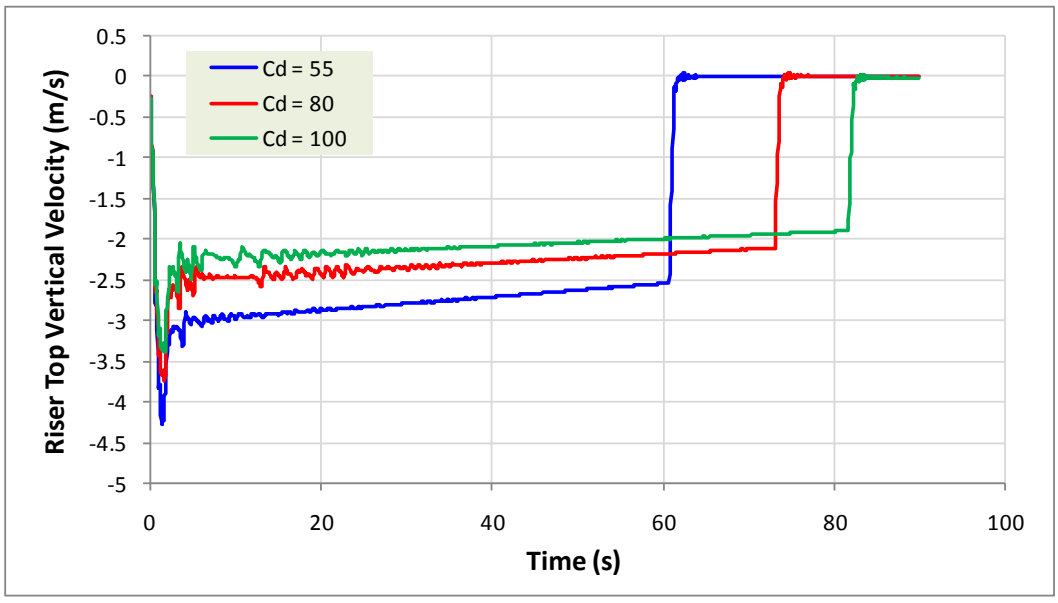

Figure 14 Time Histories of Vertical Velocity at Riser Top with Different Damper Drag

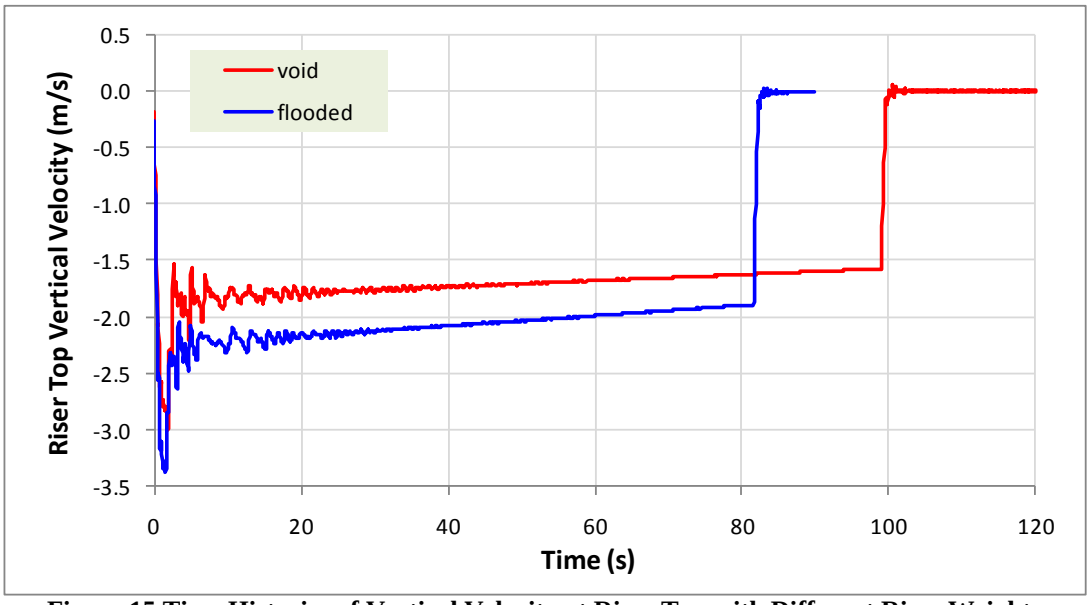

Figure 15 Time Histories of Vertical Velocity at Riser Top with Different Riser Weight

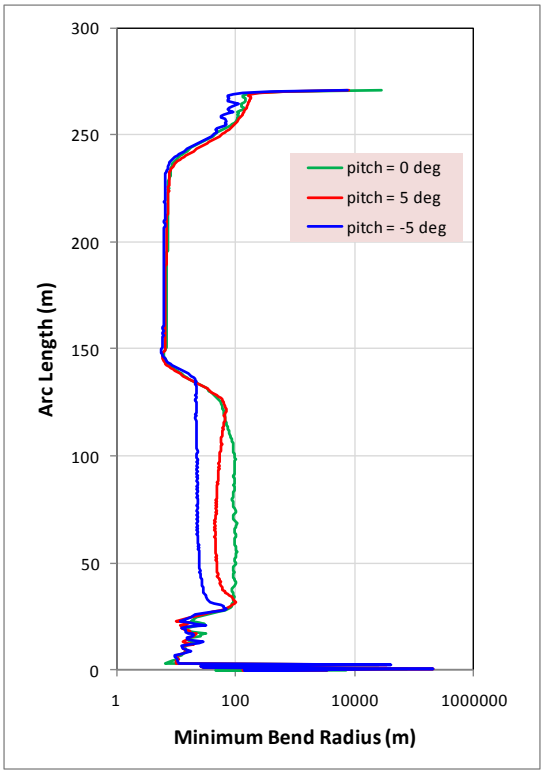

Figure 16 Riser MBR Variation with Platform Pitch

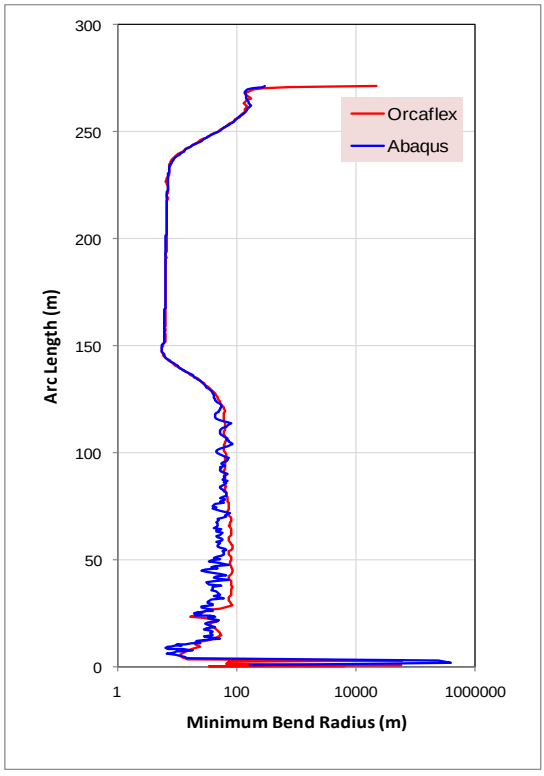

Figure 17 Comparison of Minimum Bend Radius

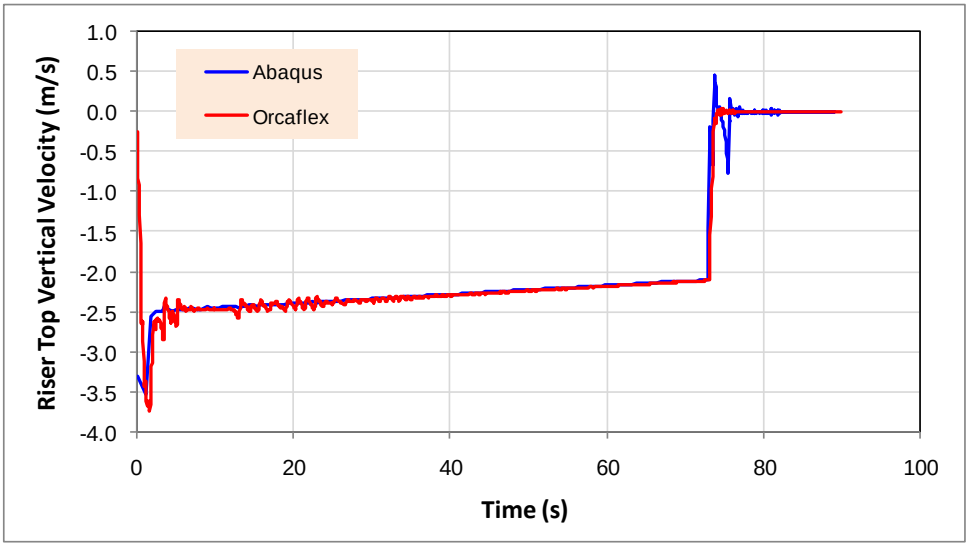

Figure 18 Comparison of Riser Top Vertical Velocity